COMPRESSIVE-TO-TENSILE STRENGTH RATIO OF BUCKLING-RESTRAINED BRACES USING STEEL-AND-MORTAR PLANKS

T. WAKAYAMA[1*], T. OURA[2†], M. MIDORIKAWA[3], M. IWATA[4], R. IIZUKA[5], M. MURAI[6], and T. ASARI[7]

[1] *Kajima Corp., M. Eng.* (*Formerly Graduate Student of Hokkaido University*), *Japan*
[2] *Graduate Student, Graduate School of Engrg., Hokkaido University, Japan*
[3] *Prof., Faculty of Engrg., Hokkaido University, Dr. Eng., Japan*
[4] *Prof., Dept. of Architecture and Building Engrg., Kanagawa University, Japan*
[5] *Graduate Student, Dept of Architecture and Building Engrg., Kanagawa University, Japan*
[6] *Formerly Technician, Dept. of Architecture and Building Engrg., Kanagawa University*
[7] *Asst. Prof., Faculty of Engrg, Hokkaido University, Dr. Eng., Japan*

ABSTRACT

A buckling-restrained brace (BRB) is composed of a steel core, which resists axial force, and a buckling-restraining system. A carefully designed clearance, often filled with unbonded material, is placed between the steel core and the restraining system to avoid force transfer between the two components through friction. Consequently, BRBs are able to provide stable hysteresis characteristics with the same strength in tension and compression.

The authors have developed a new variation of BRBs that use steel-and-mortar planks for the buckling-restraining system. The key advantage of these BRBs is that quality control can be achieved easily. A large number of laboratory test results suggest that the BRBs using steel-and-mortar planks exhibit excellent performance on par with widely used commercialized BRB products.

This paper reports recent findings from the research and development effort towards developing reliable and economic BRBs. The emphasis is on the buckling deformation of the steel core and force transfer between the steel core and the buckling-restraining system. Static, cyclic loading tests were performed on six BRBs using four different slenderness ratios for the steel core. The newly obtained data was combined with past data to refine the compressive-to-tensile strength ratio equation to account for the distribution of axial force along the length of the steel core.

Keywords: Buckling-restrained brace, Compressive-to-tensile strength ratio, Cyclic loading test, Slenderness ratio, Friction force.

---

[*] Presenter: Email: wakabo220@gmail.com

[†] Corresponding author: Email: takumi-0609@frontier.hokudai.ac.jp

1. INTRODUCTION

Buckling-restrained braces (BRBs) are implemented in building structures as devices that control their seismic response. In a structure that implements BRBs, the beams and columns are protected from the seismic damage as compared to a conventional structure. In such a damage-controlled structure, the continuous use of an entire building without the need for demolition is enabled through the replacement of only the BRBs. The use of BRBs can result in significant economic and global environmental benefits including reduction of industrial waste.

The authors have proposed and developed BRBs that use steel-and-mortar planks (a pair of mortar-filled steel channels forming a tube by welding) for the buckling-restraining system. A large number of cyclic loading tests have demonstrated that these BRBs exhibit stable hysteretic behavior under high cyclic strain (Iwata & Murai 2006, Midorikawa et al. 2010, Midorikawa et al. 2011). The test data was utilized to develop design equations for the compressive-to-tensile strength ratio of the BRBs (Midorikawa et al. 2010). However, the original equation does not reflect the observation that, when in compression, the axial force decreases from the ends toward the middle of the yielding segment. This is because part of the axial force is transferred to the buckling-restraining system through friction acting between the steel core and mortar.

In this paper, the compressive-to-tensile strength ratio of BRB is examined by cyclic loading tests. Six specimens were tested which four different slenderness ratios of the yielding segment. Subsequently, the design equation for compressive-to-tensile strength ratio was improved to reflect the distribution of axial force in the steel core.

2. TEST PROGRAM

2.1. Test specimens

Figure 1 illustrates the dimensions of the specimens. As shown in Figure 1, unbonded material, 1.0-mm thick butyl rubber, was applied along the entire surface of the steel core to create clearance between the steel core and the mortar.

Material properties established from the steel core and the mortar are listed in Tables 1 and 2. Table 3 lists the test specimens. The material grade of the steel core is SN400B, and that of the buckling-restraining system is SS400. The value of P_E/P_y listed in Table 3 is an indicator of the restraining force required to ensure stable energy dissipation of the BRBs, where P_E is the buckling load of the buckling- restraining system and P_y is the yield strength of the steel core. Four different slenderness ratio settings of 520, 560, 600 and 750 were adopted for the yielding segment. The ‘S’ in the specimen name indicate that strain gauges were densely attached to the steel core.

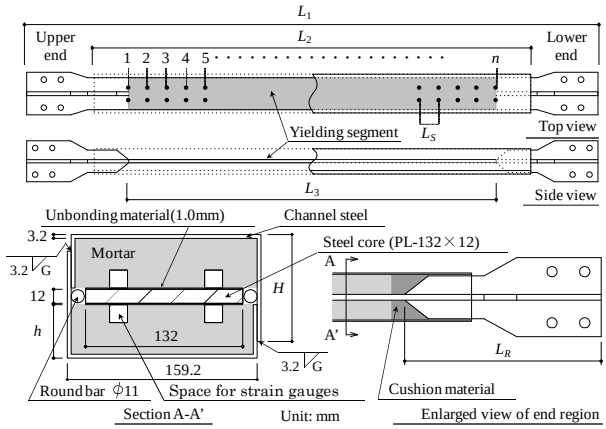

Figure 1: Test specimens

Table 1: Mechanical properties of steel core

Yield stress (N/mm^2)	Tensile strength (N/mm^2)	Yield to tensile ratio (%)	Yield strain (%)
312	451	69.5	0.171

Table 2: Mechanical properties of mortar

Specimen	Compressive strength (N/mm^2)	Young's modulus (N/mm^2)
L520, L560	60.1	16700.0
L560S, L600	69.7	17000.0
L750, L750S	65.4	13600.0

Table 3: List of test specimens

Specimen	Steel core					Restraining system				Strain gauges	
	λ	L_1 (mm)	L_2 (mm)	L_3 (mm)	P_y (kN)	Cross section	$I\times10^4$ (mm^4)	P_E (kN)	P_E/P_y	n	L_S (mm)
L520	518	2634	2078	1794	494	C-159.2×50×100×3.2	475	1386	2.80	--	--
L560	559	2775	2215	1935		C-159.2×52.5×105×3.2	529	1389	2.81	--	--
L560S										37	53.8
L600	600	2917	2353	2077		C-159.2×55×110×3.2	585	1392	2.82	--	--
L750	763	3482	2900	2642		C-159.2×64.5×129×3.2	836	1396	2.82	--	--
L750S										49	55.0

Notes) Core plate: Cross section = PL-132×12, Cross sectional area = 1584(mm^2), Width-to-thickness ratio = 11.0

2.2. Test setup, Loading protocol and Measurement

Figure 2 illustrates the test setup. Static loading was applied by controlling the axial deformation of the yielding segment of the steel core, δ. The yielding segment was elongated and contracted according to the loading protocol shown in Table 4.

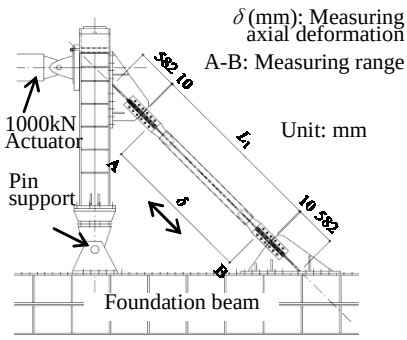

Figure 2: Test setup

Table 4: Loading protocol

Axial strain amplitude (%)	Loading cycles
$\varepsilon_y/3$	1
$2\varepsilon_y/3$	1
0.25	1
0.50	2
0.75	2
1.00	5
1.50	2
2.00	2
2.50	2
3.00	--

3. TEST RESULTS AND DISCUSSION

3.1. Hysteretic characteristics

The relationship between the normalized axial force, P/P_y, which is obtained by dividing the axial load, P, by P_y, and the axial strain, ε, for each specimen is shown in Figure 3. All specimens exhibited stable hysteresis up to a high strain amplitude range of 3.0%. A slight strength increase in compression observed in the amplitude of 3.0% in Specimen L750 was due to the fin stiffeners at

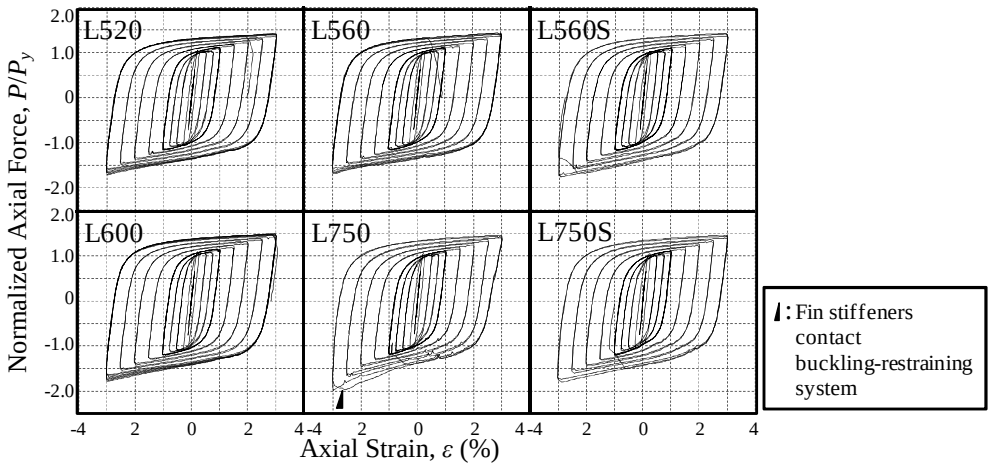

Figure 3: P/P_y - ε(%) relationship

the end of the steel core contacting the buckling-restraining system.

3.2. Failure mode of test specimens

Table 5 summarizes the observations from each specimen, such as the final half cycle, i.e., the strain amplitude when the load bearing capacity started to decline, the failure modes identified after the test was completed, and the buckling mode number, i.e., the number of half-waves counted along the length of the yielding segment. Three specimens (L560S, L750, and L750S) exhibited local buckling about the weak-axis of the yielding segment, and the remaining three specimens (L520, L560, and L600) failed due to tensile fracture of the yielding segment. Mild buckling deformation about the strong-axis was observed in all specimens excluding L600 during the high amplitude of 3.0%.

Table 5: Test results and observations

Specimen	Final half cycle	Failure mode	Buckling mode number, M
L520	7th (-) ±3.0% cycle	Tensile fracture*	23
L560	6th (-) ±3.0% cycle	Tensile fracture*	27
L560S	3rd (+) ±3.0% cycle	Local buckling about weak-axis near lower end*	22
L600	8th (-) ±3.0% cycle	Tensile fracture	32
L750	3rd (+) ±3.0% cycle	Local buckling about weak-axis at upper end*	34
L750S	3rd (+) ±3.0% cycle	Local buckling about weak-axis at lower end*	30

Note) *: Mild buckling deformation about strong-axis occurred at high axial strain.

3.3. Strength increase factor

Figure 4 illustrates the relationship between the strength increase factor, P_c/P_y and P_t/P_y, and the axial strain amplitude, where P_c and P_t are the compressive strength and tensile strength, respectively, obtained at that amplitude. At the largest amplitude of 3.0%, the value of P_t/P_y was 1.4 in all specimens. On the other hand, the value of P_c/P_y varied between specimens: 1.6 in L520, L560, and L600; and 1.7 in L560S and L750S. Consequently, the larger the slenderness ratio was, the greater the strength increase factor was in compression. Specimen L750 developed an extraordinary P_c/P_y at the amplitude of 3.0 %. This was due to the fin stiffeners at the end of the steel core contacting the buckling-restraining system, as mentioned in Section 3.1.

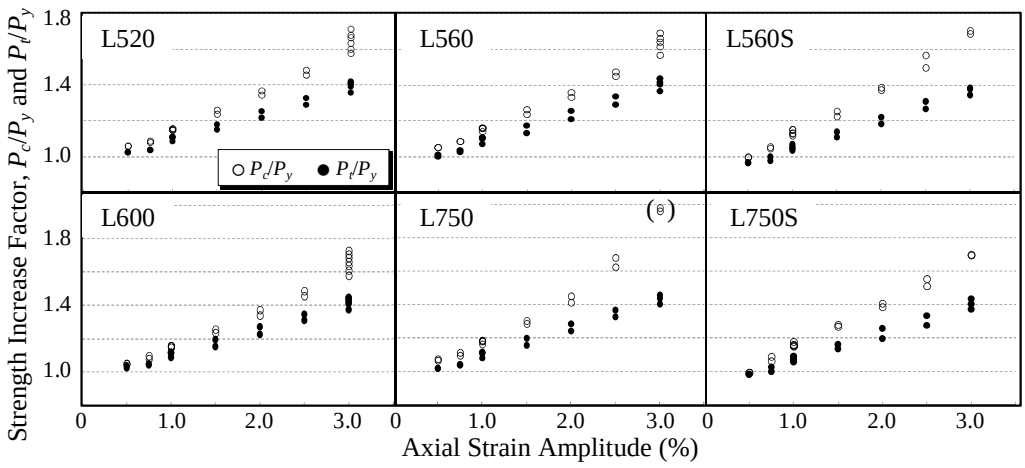

Figure 4: Relationship between P_c/P_y, P_t/P_y and axial strain amplitude

3.4. Evaluation formula of buckling mode number

In an earlier study (Midorikawa at al. 2010), two formulae for the buckling mode number, M, of the BRBs was proposed.

$$M_1 = \frac{\lambda}{\pi}\sqrt{\frac{\sigma_y P_c / P_y}{E_r}}\ ,\quad M_2 = \frac{\lambda}{\pi}\sqrt{\frac{\sigma_y}{E}}\left(\sqrt{\frac{P_c / P_y - 1}{E_r / E}} + 1\right) \tag{1, 2}$$

In the above equations, λ is the slenderness ratio of the yield segment, E is the Young's modulus of the steel core, and E_r is as follows.

$$E_r = \frac{4EE_t}{\left(\sqrt{E_t} + \sqrt{E}\right)^2} \tag{3}$$

The tangent modulus, E_t, was set equal to $0.03E$ based on calibration to the test results.

Figure 5 compares the buckling mode number estimated by Eqns. (1) and (2) and the values observed from the test. During the test, strain gauge measurements were used to count the number

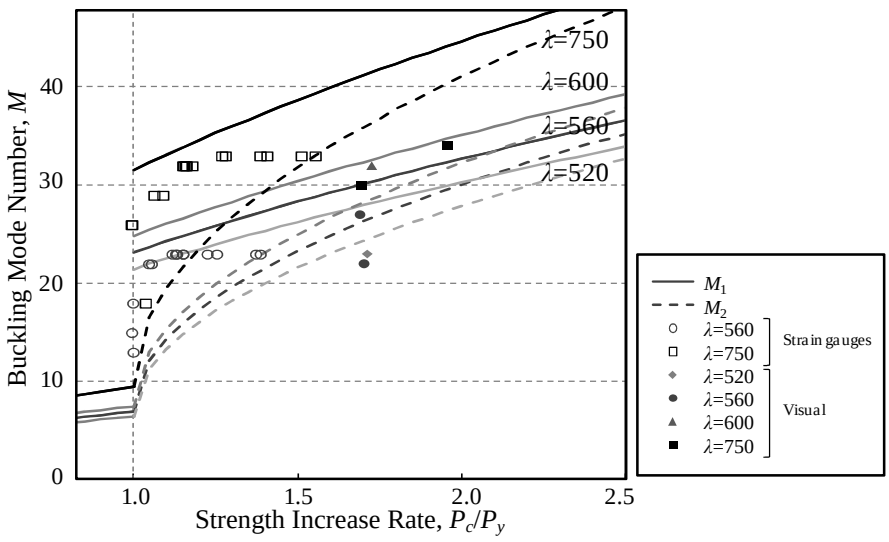

Figure 5: M - P_c/P_y relationship

of inflection points. After the test, the specimens were taken apart for visual inspection. The observed values increased sharply in the range of P_c/P_y=1.0 to 1.2 but remained rather constant afterwards. The ultimate values are closer to the estimates by Eqn. (2). It should be noted that Eqn. (1) provides an upper limit to the observed buckling mode number from the test results. Similar trends between estimation and test results have been reported in the earlier study.

3.5. Compressive-to-tensile strength ratio

In a more recent study (Midorikawa at al. 2011), the relationship between the slenderness ratio, λ, and the compressive-to-tensile strength ratio, P_c/P_t, is obtained by the following Eqn. (4), where μ is the friction coefficient, S is the buckling mode amplitude, and L_m is the half-wave length of buckling mode shape.

$$\frac{P_c}{P_t} = \frac{A_c}{A_t} \cdot \frac{1+\mu(S/L_m)}{1-\mu(2M-1)(S/L_m)} \tag{4}$$

Eqn. (4) neglects the variation of compressive force along the length of the steel core, and assumes that the restraining force, B, is the same at every contact point. However, test observations suggest that the axial strain decreases from the ends toward the middle of the yielding segment. Consequently, the relationship between λ and P_c/P_t is further examined to derive a modified design equation. First, P_c/P_t is expressed as follows.

$$\frac{P_c}{P_t} = \frac{A_c}{A_t} + \frac{F}{P_t} \tag{5}$$

During yielding of the BRB, the change in volume of the yielding segment might be neglected to give a Poisson's ratio ν=0.5. The ratio of sectional area in compression, A_c, and in tension, A_t, is expressed as follows.

$$\frac{A_c}{A_t} = \frac{(1+0.5\varepsilon_x)^2}{(1-0.5\varepsilon_x)^2} \tag{6}$$

Figure 6 illustrates deformation of the steel core under high mode buckling. The second and third half-waves from the left end are expressed in free-body diagrams. Expressions for the restraining forces B_{12} and B_{23} are obtained from equilibrium. The change in axial force between these two half-waves is expressed in Eqn. (7).

$$P_2 = \frac{L_{12}-\mu S}{L_{12}+\mu S} P_1 \tag{7}$$

Similar equations can be established from the end to the fixed point, i.e., the point where the no relative motion occurs between the steel core and the buckling-restraining system, typically located in the middle of the yielding segment. At the fixed point, the compression is P_n and restraining force is $B_{n(n+1)}$.

$$P_n = \frac{L_{(n-1)n}-\mu S}{L_{(n-1)n}+\mu S} P_{n-1}, \quad B_{n(n+1)} = \frac{P_n S}{L_{n(n+1)}+\mu S} \tag{8, 9}$$

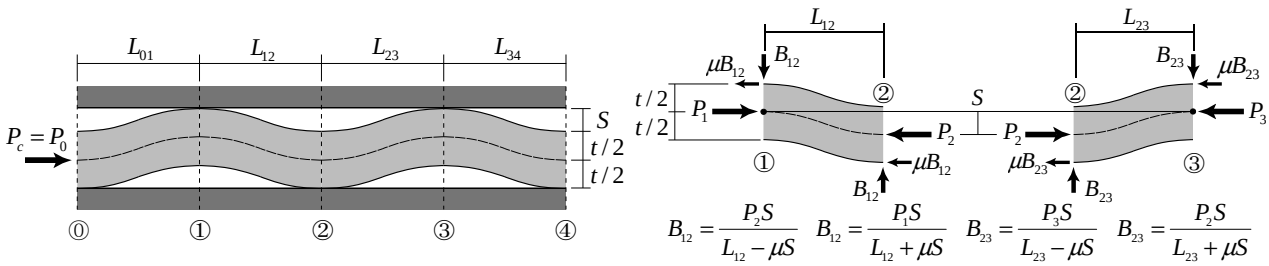

Figure 6: Deformation of higher mode buckling of steel core

Consequently, the total friction force, F, which is the compression that is ultimately resisted by the buckling-restraining system, is expressed as follows.

$$F = 2\mu \sum B_{n(n+1)} \tag{10}$$

When the half-wave length of the buckling mode shape is constant, P_n, $B_{n(n+1)}$, and F can be obtained as follows.

$$P_n = R^n \cdot P_0 \quad \left(R = \frac{1-\mu(S/L_m)}{1+\mu(S/L_m)} \le 1 \right) \tag{11}$$

$$B_{n(n+1)} = \frac{P_n S}{L_m + \mu S}, \quad F = 2\mu \sum_{n=0}^{M/2} B_{n(n+1)} = \frac{2\mu S}{L_m + \mu S} P_0 \sum_{n=0}^{M/2} R^n = P_0 \left(1 - R^{M/2+1}\right) \tag{12, 13}$$

Finally, the expression for P_c/P_t, is obtained by substituting Eqn. (13) into Eqn. (5).

$$\frac{P_c}{P_t} = \frac{A_c}{A_t} \cdot \frac{1}{R^{M/2+1}} \tag{14}$$

It is conceivable that the fixed point may be in the middle during the earlier phase of the cyclic loading test, but that the fixed point moves close to the end of the buckling-restraining system. Test observations suggest that the studs that anchor the yielding segment to the mortar of the buckling-restraining system can become ineffective during high amplitude cycles after the mortar fails by bearing or a stronger bearing point forms at the end of the buckling-restraining system. When the fixed point is formed at the end of the buckling-restraining system, P_c/P_t is expressed as follows.

$$\frac{P_c}{P_t} = \frac{A_c}{A_t} \cdot \frac{1}{R^{M+1}} \tag{15}$$

Figure 7 shows the relationships between P_c/P_t and the axial strain amplitude, comparing the values estimated by Eqns. (14) and (15) against the test values measured from the tests. Three specimens, L520, L560, and L600, which failed due to tensile fracture, are in good agreement with Eqn. (14). It is conceivable that in these specimens, the fixed point remained at the middle of the steel core until the end of the test. The value of P_c/P_t increase gradually with strain amplitude up to the final 3.0%. In the remaining three specimens, L560S, L750, and L750S, the P_c/P_t values were either close to Eqn. (15) or between Eqns. (14) and (15). This result is likely due to the fixed point, which was

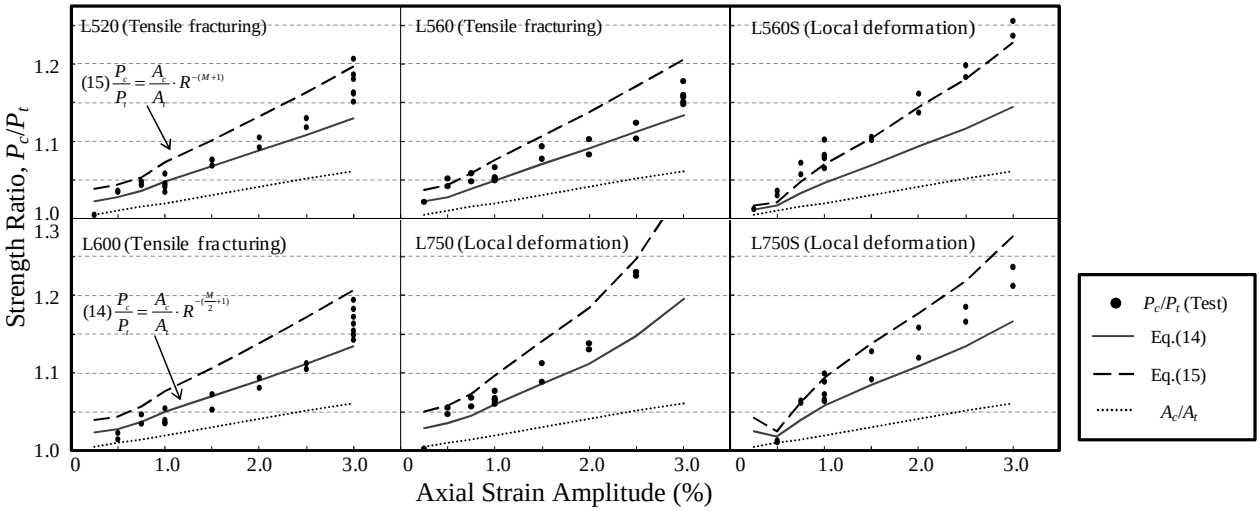

Figure 7: Relationship between strength ratio, P_c/P_t and axial strain amplitude

originally at the middle of the steel more, shifting position towards the end of the buckling-restraining system.

4. CONCLUSIONS

Equation (1) provides an upper limit to the buckling mode number measured from the test results. This finding is consistent with previous studies.

The compressive-to-tensile strength ratio, P_c/P_t, increase in proportion to the slenderness ratio of the yield segment. Equations (14) and (15) provide a reasonable estimate of P_c/P_t considering the distribution of friction forces between the steel core and the restraining mortar.

5. ACKNOWLEDGMENTS

The authors would like to acknowledge Prof. T. Okazaki, Hokkaido Univ., Ph.D. for his valuable discussion and comments.

REFERENCES

Iwata, M. and Murai, M. (2006). Buckling-restrained brace using steel mortar planks; performance evaluation as a hysteretic damper. *Earthquake Engineering and Structural Dynamics* **35:14**, 1807-1826.

Midorikawa, M., Sasaki, D., Asari, T., Murai, M. and Iwata, M. (2010). Experimental study on buckling-restrained braces using steel mortar planks-Effects of the clearance between core plate and restraining member on compressive strength and estimation of the number of buckling mode related to compressive strength-. *Journal of Structural and Construction Engineering*, AIJ **75:653**, 1361-1368 (in Japanese).

Midorikawa, M., Tanaka, Y., Otake, T., Asari, T., Murai, M. and Iwata, M. (2011). Experimental study on buckling-restrained braces using steel mortar planks-Evaluation of the buckling mode number and the relationship between strength ratio and slenderness ratio-. *Journal of Structural and Construction Engineering*, AIJ **76:664**, 1153-1160 (in Japanese).